KYUNGPOOK Math. J. 61(2021), 323-351
https://doi.org/10.5666/KMJ.2021.61.2.323
pISSN 1225-6951 eISSN 0454-8124

MHD Pulsatile Flow and Heat Transfer of Two Immiscible Couple Stress Fluids Between Permeable Beds

Deepak Kumar* and Manju Agarwal
Department of Mathematics and Astronomy, University of Lucknow, Lucknow, U.P., India, Pin-226007
e-mail : deepakpatel0412@gmail.com *and* manjuak@yahoo.com

Abstract. The present paper addresses magnetohydrodynamic pulsating flow and heat transfer of two immiscible, incompressible, and conducting couple stress fluids between two permeable beds. The flow between the permeable beds is assumed to be governed by Stokes' [28] couple stress fluid flow equations, whereas the dynamics of permeable beds is determined by Darcy's law. In this study, matching conditions were used at the fluid–fluid interface, whereas the B-J slip boundary condition was employed at the fluid–porous interface. The governing equations were solved analytically, and the expressions for velocity, temperature, mass flux, skin friction, and rate of heat transfer were obtained. The analytical expressions were numerically evaluated, and the results are presented through graphs and tables.

1. Introduction

Multiphase flow in porous channels and heat transfer have been studied more and more recently. This research area has large-scale potential in engineering and geophysical applications. Some major applications of such flows are in agricultural engineering for studying surface and underground water flows [10], in nuclear engineering for designing pebble bed reactors, in the petroleum industry for studying the flow of hydrocarbons in reservoir rocks, and in geotechnical engineering for underground waste disposal. Other applications include infiltration of water, sewage, porous bearings, solid matrix heat exchangers, and bioconvection in porous media. Many researchers [5, 8, 21] have considered blood flow as a two-phase flow.

Vajravelu et al. [32] analysed the hydromagnetic unsteady flow of two conduct-

* Corresponding Author.
Received May 27, 2017; revised August 19, 2018; accepted August 20, 2018.
2010 Mathematics Subject Classification: 76S99, 76T99, 76A05.
Key words and phrases: couple stress fluid, permeable bed, Darcy's law, Beaver-Joseph slip condition.

Nomenclature

α	Slip parameter	K_2	Permeability of the upper permeable bed
ϵ_i	Porosity parameter, $\frac{h}{\sqrt{K_i}}$	k_i	Thermal conductivity of the fluid
η'	Couple stress viscosity ratio, $\frac{\eta_2}{\eta_1}$	M	Hartmann number, $B_o h\sqrt{\frac{\sigma_1}{\mu_1}}$
η_i	Couple stress viscosity	Pr	Prandtl number, $\frac{\mu_1 C_p}{k_1}$
μ'	Viscosity ratio, $\frac{\mu_2}{\mu_1}$	Ri	Reynolds number, $\frac{\rho_i u h}{\mu_i}$
μ_i	Viscosity of the fluid	S_i	Couple stress parameter, $\frac{\mu_i h^2}{\eta_i}$
ω	Frequency	t	Time
ρ'	Density ratio, $\frac{\rho_2}{\rho_1}$	T_{w_1}	Temperature at the lower permeable bed
ρ_i	Density of the fluid	T_{w_2}	Temperature at the upper permeable bed
σ'	Electric conductivity ratio, $\frac{\sigma_2}{\sigma_1}$	u	Average velocity
σ_i	Electric conductivity of the fluid	u_i	Velocity in x-direction
θ_i	Non dimensional temperature	x, y	Coordinates along the channel
C_p	Specific heat at constant pressure		
Ec	Eckert number, $\frac{u^2}{C_p(T_{w_2}-T_{w_1})}$		
k'	Thermal conductivity ratio, $\frac{k_2}{k_1}$		
K_1	Permeability of the lower permeable bed		

ing immiscible fluids between two permeable beds with different permeabilities. They obtained expressions for interface velocity, velocity distribution, and mass flow rate. Subsequently, they analysed the pulsatile flow of a viscous fluid between two permeable beds using Darcy's law [33]. Analytical solutions of a flow in a porous medium inside permeable beds under an exponentially decaying pressure gradient were obtained by Prasad and Kumar [18]. Jogie and Bhatt [13] studied the laminar flow of two immiscible and incompressible fluids through permeable channels by using the B-J slip condition. Panda et al. [17] studied the three-layer fluid flow in a channel with a small obstruction on an impermeable bottom. Umavathi et al. [31] studied the unsteady flow in a porous medium sandwiched between viscous fluids. In the case of flow through porous mediums, Beavers and Joseph [3] demonstrated experimentally that the usual no-slip boundary condition is no longer valid for a fluid–porous boundary. They postulated the existence of slip at the fluid–porous boundary resulted in a condition called B-J slip. According to this condition, the Poiseuille velocity in a channel and Darcy's velocity in the porous medium can be coupled using the following equation:

$$\frac{\partial u_f}{\partial y} = \frac{\alpha}{K^{\frac{1}{2}}}(u_f - u_m).$$

Here, the clear fluid region occupies the region ($y > 0$), u_f is the fluid velocity, and u_f and $\frac{\partial u_f}{\partial y}$ are evaluated at $y = 0+$. The Darcy velocity u_m is evaluated at some small distance below $y = 0$. The Beaver–Joseph constant α is dimensionless and depends on the structure of the porous medium and independent of the fluid viscosity and permeability.

Flow rheology is the main principle of lubrication theory. Two main theories explain the flow of liquids: classical continuum mechanics, which neglects the effects of fluid particle size, and microcontinuum mechanism, which accounts for the intrinsic motion of material particles (e.g. polymer molecules in a polymer suspension). Further, to study the discriminative behaviour of the fluids containing substructures such as polymer fluids, many theories of microcontinuum have been developed [1, 2, 28, 29]. Stokes [28] presented a simple generalisation of the classical theory of fluids, which allows for polar effects such as the presence of an antisymmetric stress tensor, couple stresses, and body couples. Couple stresses arise in fluids containing additives with large molecules. Major applications of couple stress fluid models include pumping fluids such as colloidal fluids, synthetic lubricants, liquid crystals, and biofluids (e.g. blood [26, 27]). Many researchers have applied the couple stress fluid model on lubrication problems such as squeeze film bearings [4, 20], thrust bearings [9, 14], and journal bearings [6, 16].

Soundalgekar and Aranake [23] studied the effects of couple stress on the magnetohydrodynamic Couette flow of a conducting fluid between two parallel plates. They concluded that current density is significantly affected by small values of couple stress parameter, and skin friction is affected by couple stress in the presence of a magnetic field. A brief discussion on the theory of microstructure fluids can be found in [29]. Szen and Rajagopal [30] analysed the flow of a non-Newtonian fluid between heated plates and obtained expressions by using constant and variable viscosity models. Recently, Siddiqui et.al. [22] studied Couette and Poiseuille flow of two non-Newtonian fluids, namely a fourth-grade fluid and Sisko fluid and concluded that solutions of the Newtonian and fourth-grade fluids can be recovered by substituting $n = 0$ and 3 in Sisko model solutions. Islam and Zhou [11] derived exact solutions for the two-dimensional flow of couple stress fluids by using the inverse method. Farooq et al. [7] studied the non isothermal flow of a couple stress fluid with variable viscosity between two parallel plates. Iyengar and Bitla [12] investigated the pulsating flow of a couple stress fluid between permeable beds through constant injection and suction. Subsequently, Bitla and Iyengar [19] studied the oscillatory flow of a couple stress fluid inside permeable beds in the presence of a uniform magnetic field. Srinivas et al. [24] analysed entropy generation by the flow of two immiscible couple stress fluids between porous beds. The effects of Hall currents on the thermal instability of a compressible couple stress fluid in the presence of a horizontal magnetic field were investigated by Mehta et al. [15]. Srinivas and Murthy [25] studied the flow of two immiscible couple stress fluids between permeable beds and concluded that the presence of the couple stress reduces the flow velocity.

In view of the various applications of couple stress fluid flow in natural systems (e.g. in ground water flow, where multiple layers of fluids are present between permeable soil layers), human systems, and many engineering problems (e.g. in the petroleum industry to study the flow of many immiscible hydrocarbons between porous rocks), we analysed an MHD pulsating flow and heat transfer of two immiscible, incompressible, and conducting couple stress fluids between two permeable beds. The effects of different flow parameters on velocity and temperature profiles are displayed graphically and those on shear stress and heat transfer rates at permeable beds are presented numerically through tables.

2. Problem Statement

Consider the flow of two electrically conducting immiscible couple stress fluids in a channel of height $2h$ bounded by two permeable beds. Permeable beds have infinite thicknesses with varying permeabilities. The permeabilities of lower and upper permeable beds are K_1 and K_2, respectively. The flow geometry is presented in Fig. 1. The origin is the centre of the channel, and X and Y are horizontal and vertical coordinates, respectively. The region I $(-h \preceq y \preceq 0)$ is occupied by an electrically conducting couple stress fluid of density ρ_1, viscosity μ_1, electric conductivity σ_1, and thermal conductivity k_1. The region II $(0 \preceq y \preceq h)$ is filled with an electrically conducting couple stress fluid of density $\rho_2(\prec \rho_1)$, viscosity μ_2, electric conductivity σ_2, and thermal conductivity k_2. The lower and upper permeable beds are held at different constant temperatures T_{w_1} and T_{w_2}, respectively, with $T_{w_2} \succ T_{w_1}$. The field equations describing a couple stress fluid are similar to

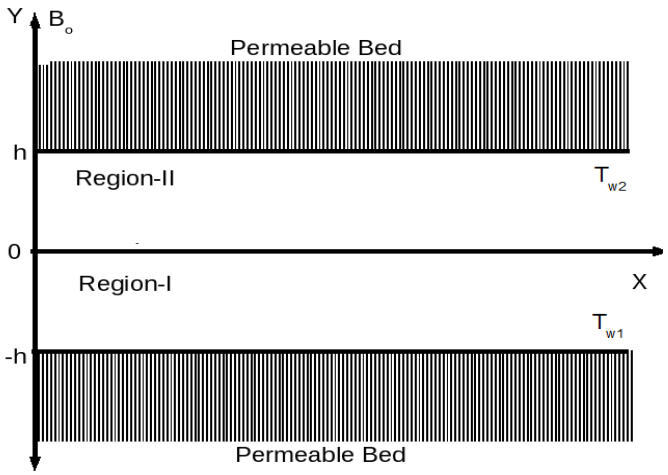

Figure 1: Schematic of flow

Navier–Stokes equations and are given by:

Conservation of mass

$$\frac{\partial \rho}{\partial t} + \bigtriangledown.(\rho \overrightarrow{q}) = 0. \tag{2.1}$$

Conservation of momentum

$$\begin{aligned} \rho \frac{d\overrightarrow{q}}{dt} =& - \bigtriangledown P + \rho \overrightarrow{f} + \frac{1}{2} \bigtriangledown \times (\rho \overrightarrow{l}) + \bigtriangledown \times (\bigtriangledown \times (\overrightarrow{q})) \\ & - \eta \bigtriangledown \times (\bigtriangledown \times (\bigtriangledown \times (\bigtriangledown \times \overrightarrow{q}))) + (\lambda + 2\mu) \bigtriangledown (\bigtriangledown.(\overrightarrow{q})). \end{aligned} \tag{2.2}$$

Conservation of energy

$$\rho \frac{dE}{dt} = \tau_{ij} D_{rs} + \left(m_{rs} - \frac{1}{3} m_{rr} \delta_{rs} \right) \omega_{s,r} - h_{r,r} + \rho \xi. \tag{2.3}$$

Following Stokes, the constitutive equations of couple stress fluid are:

$$\tau_{ij} = -P\delta_{ij} + \lambda \bigtriangledown .(\overrightarrow{q})\delta_{ij} + 2\mu d_{ij} + \frac{1}{2} \epsilon_{i,jk} [m_{,i} + 4\eta w_{k,rr} + \rho c_k] \tag{2.4}$$

$$m_{ij} = \frac{1}{3} m \delta_{ij} + 4\eta w_{j,i} + 4\eta^{'} w_{i,j}, \tag{2.5}$$

where material constants λ and μ are the viscosity coefficients and η and $\eta^{'}$ are the couple stress viscosity coefficients, which satisfy the constraints $\mu \succeq 0, 3\lambda + 2\mu \succeq 0, \eta \succeq 0$, and $\mid \eta^{'} \mid \preceq \eta$. $\sqrt{\frac{\eta}{\mu}}$ is the length parameter, which represents the characteristic measure of the polarity of the couple stress fluid and is identically zero for non polar fluids.

The scalar quantities P and ρ denote pressure at any point in the fluid and density of the fluid, respectively. The vectors $\overrightarrow{q}$, ω, $\overrightarrow{f}$, and $\overrightarrow{l}$ are the velocity, vorticity, body force per unit mass, and body couple per unit mass, respectively. The tensors τ_{ij} and m_{ij} are force stress tensor and couple stress tensor, respectively. δ_{ij} is the Kronecker symbol, d_{ij} is the component of the rate of shear strain, ρc_k is body couple vector, $w_{i,j}$ is the spin tensor, and $\epsilon_{i,jk}$ is the Levi–Civita symbol. D_{rs} is the deformation tensor, which is equal to the symmetric part of the velocity gradient. E is the internal energy density per unit area, h_i is the influx of energy per unit area, q is the internal energy source density per unit area, and the comma denotes covariant differentiation.

Flow in both regions is assumed to be one-dimensional, laminar, and driven only by a pulsatile pressure gradient applied at the inlet of the channel. Assuming the permeable beds to be homogeneous and of infinite thickness so that Darcy's law can be applied with B-J slip condition at the fluid–porous interface, the velocity and temperature distribution in the channel are given by:

2.1. Velocity Distribution

The governing equation in Region I is

$$\rho_1 \frac{\partial u_1}{\partial t} = -\frac{\partial p}{\partial x} + \mu_1 \frac{\partial^2 u_1}{\partial y^2} - \eta_1 \frac{\partial^4 u_1}{\partial y^4} - \sigma_1 B_o^2 u_1. \tag{2.6}$$

The governing equation in Region II is

$$\rho_2 \frac{\partial u_2}{\partial t} = -\frac{\partial p}{\partial x} + \mu_2 \frac{\partial^2 u_2}{\partial y^2} - \eta_2 \frac{\partial^4 u_2}{\partial y^4} - \sigma_2 B_o^2 u_2. \tag{2.7}$$

To determine velocities u_1 and u_2, we adopt the following boundary and interface conditions:

1. At the lower fluid–porous boundary, couple stress disappears (i.e. no spin exists) and B-J slip condition is considered:

$$\frac{\partial^2 u_1}{\partial y^2} = 0 \qquad \text{at } y = -h \tag{2.8}$$

$$u_1 = u_1^{'} \qquad \text{at } y = -h \tag{2.9}$$

$$\frac{\partial u_1}{\partial y} = \frac{\alpha}{\sqrt{K_1}}(u_1^{'} - Q_1) \qquad \text{at } y = -h. \tag{2.10}$$

2. At the fluid–fluid interface, velocity, rotation, shear stress, and couple stress are continuous:

$$\left\{ \begin{array}{c} u_1 = u_2,\ \frac{\partial u_1}{\partial y} = \frac{\partial u_2}{\partial y},\ \mu_1 \frac{\partial u_1}{\partial y} - \eta_1 \frac{\partial^3 u_1}{\partial y^3} = \mu_2 \frac{\partial u_2}{\partial y} - \eta_2 \frac{\partial^3 u_2}{\partial y^3},\ \\ \eta_1 \frac{\partial^2 u_1}{\partial y 2} = \eta_2 \frac{\partial^2 u_2}{\partial y 2} \end{array} \right\} \text{at } \ y = 0. \tag{2.11}$$

3. At the upper fluid–porous boundary, couple stress disappears (i.e. no spin exists) and B-J slip condition is considered:

$$\frac{\partial^2 u_2}{\partial y^2} = 0 \qquad \text{at } y = h \tag{2.12}$$

$$u_2 = u_2^{'} \qquad \text{at } y = h \tag{2.13}$$

$$\frac{\partial u_2}{\partial y} = -\frac{\alpha}{\sqrt{K_2}}(u_2^{'} - Q_2) \qquad \text{at } y = h, \tag{2.14}$$

where u_1 and u_2 are velocities in Regions I and II, respectively, and B_o is the applied magnetic field normal to the flow direction. $Q_1 = -\frac{K_1}{\mu_1}\frac{\partial p}{\partial x}$ and $Q_2 = -\frac{K_2}{\mu_2}\frac{\partial p}{\partial x}$ are Darcy velocities in Regions I and II, respectively. $\frac{\partial p}{\partial x}$ is the pulsatile pressure gradient given by:

$$-\frac{\partial p}{\partial x} = \left(\frac{\partial p}{\partial x}\right)_s + \left(\frac{\partial p}{\partial x}\right)_o e^{i\omega t},$$

where $\left(\frac{\partial p}{\partial x}\right)_s$ and $\left(\frac{\partial p}{\partial x}\right)_o$ represent the steady and oscillatory parts of pulsatile pressure gradient, respectively, and ω is the frequency.

2.2. Temperature Distribution

The governing equation in Region I is

$$\rho_1 C_p \frac{\partial T_1}{\partial t} = k_1 \frac{\partial^2 T_1}{\partial y^2} + \mu_1 \left(\frac{\partial u_1}{\partial y}\right)^2 + \eta_1 \left(\frac{\partial^2 u_1}{\partial y^2}\right)^2. \tag{2.15}$$

The governing equation in Region II is

$$\rho_2 C_p \frac{\partial T_2}{\partial t} = k_2 \frac{\partial^2 T_2}{\partial y^2} + \mu_2 \left(\frac{\partial u_2}{\partial y}\right)^2 + \eta_2 \left(\frac{\partial^2 u_2}{\partial y^2}\right)^2. \tag{2.16}$$

To determine temperature profiles T_1 and T_2, we adopt the following boundary and interface conditions:

1. At the lower permeable bed, the temperature is constant and is equal to the temperature of the lower permeable bed, that is,

$$T_1 = T_{w_1} \quad \text{at} \quad y = -h. \tag{2.17}$$

2. At the fluid–fluid interface, the temperature and heat flux are continuous, that is,

$$T_1 = T_2, \quad k_1 \frac{\partial T_1}{\partial y} = k_2 \frac{\partial T_2}{\partial y} \quad \text{at } y = 0. \tag{2.18}$$

3. At the upper permeable bed, the temperature is constant and is equal to the temperature of the upper permeable bed, that is,

$$T_2 = T_{w_2} \quad \text{at} \quad y = h, \tag{2.19}$$

where C_p is the specific heat at constant pressure.

3. Non Dimensionalization of Flow Quantities

Introducing the following non dimensional quantities

$$\left\{ \begin{array}{c} x^* = \frac{x}{h}, y^* = \frac{y}{h}, u_1^* = \frac{u_i}{u}, t^* = \frac{tu}{h}, p^* = \frac{p}{\rho_1 u^2}, \\ K_i^* = \frac{K_i}{h^2}, \omega^* = \frac{\omega}{h}, \theta_i^* = \frac{T_i - T_{w_1}}{T_{w_2} - T_{w_1}} \end{array} \right\}, \quad i = 1, 2$$

and dropping the asterisks, the velocity and temperature distributions in the non dimensional form are given as:

3.1. Velocity Distribution

Equations (2.6) and (2.7), respectively, become:

$$\frac{\partial u_1}{\partial t} = -\frac{\partial p}{\partial x} + \frac{1}{R_1}\frac{\partial^2 u_1}{\partial y^2} - \frac{1}{R_1 S_1}\frac{\partial^4 u_1}{\partial y^4} - \frac{M^2}{R_1}u_1 \tag{3.1}$$

$$\frac{\partial u_2}{\partial t} = -\frac{1}{\rho'}\frac{\partial p}{\partial x} + \frac{1}{R_2}\frac{\partial^2 u_2}{\partial y^2} - \frac{1}{R_2 S_2}\frac{\partial^4 u_2}{\partial y^4} - \frac{M^2\sigma'}{R_2\mu'}u_2. \tag{3.2}$$

The boundary and interface conditions become:

$$\frac{\partial^2 u_1}{\partial y^2} = 0 \qquad \text{at } y = -1 \tag{3.3}$$

$$u_1 = u_1^{'} \qquad \text{at } y = -1 \tag{3.4}$$

$$\frac{\partial u_1}{\partial y} = \alpha\epsilon_1\left(u_1^{'} + \frac{R_1}{\epsilon_1^2}\frac{\partial p}{\partial x}\right) \qquad \text{at } y = -1 \tag{3.5}$$

$$\left\{ \begin{array}{c} u_1 = u_2,\ \frac{\partial u_1}{\partial y} = \frac{\partial u_2}{\partial y},\ \frac{\partial u_1}{\partial y} - \frac{1}{S_1}\frac{\partial^3 u_1}{\partial y^3} = \mu'\left[\frac{\partial u_2}{\partial y} - \frac{1}{S_2}\frac{\partial^3 u_2}{\partial y^3}\right], \\ \frac{\partial^2 u_1}{\partial y 2} = \eta'\frac{\partial^2 u_2}{\partial y 2} \end{array} \right\} \text{ at } \ y = 0 \tag{3.6}$$

$$\frac{\partial^2 u_2}{\partial y^2} = 0 \qquad \text{at } y = 1 \tag{3.7}$$

$$u_2 = u_2^{'} \qquad \text{at } y = 1 \tag{3.8}$$

$$\frac{\partial u_2}{\partial y} = -\alpha\epsilon_2\left(u_2^{'} + \frac{R_2}{\epsilon_2^2\rho'}\frac{\partial p}{\partial x}\right) \qquad \text{at } y = 1, \tag{3.9}$$

where $-\frac{\partial p}{\partial x} = \left(\frac{\partial p}{\partial x}\right)_s + \left(\frac{\partial p}{\partial x}\right)_o e^{i\omega t}$ is the non dimensional pressure gradient.

3.2. Temperature Distribution

Equations (2.15) and (2.16), respectively, become:

$$\frac{\partial \theta_1}{\partial t} = \frac{1}{R_1 Pr}\frac{\partial^2 \theta_1}{\partial y^2} + \frac{Ec}{R_1}\left(\frac{\partial u_1}{\partial y}\right)^2 + \frac{Ec}{S_1 R_1}\left(\frac{\partial^2 u_1}{\partial y^2}\right)^2 \tag{3.10}$$

$$\frac{\partial \theta_2}{\partial t} = \frac{1}{R_2 Pr}\frac{k'}{\mu'}\frac{\partial^2 \theta_2}{\partial y^2} + \frac{Ec}{R_2}\left(\frac{\partial u_1}{\partial y}\right)^2 + \frac{Ec}{S_2 R_2}\left(\frac{\partial^2 u_1}{\partial y^2}\right)^2. \tag{3.11}$$

The boundary and interface conditions become:

$$\theta_1 = 0 \quad \text{at } \ y = -1 \tag{3.12}$$

$$\theta_1 = \theta_2, \quad \frac{\partial \theta_1}{\partial y} = k' \frac{\partial \theta_2}{\partial y} \qquad \text{at } y = 0 \tag{3.13}$$

$$\theta_2 = 1 \quad \text{at} \quad y = 1. \tag{3.14}$$

4. Analytical Solutions

Regarding the pulsating pressure gradient, let us assume that velocities and temperatures are in the form:

$$\left\{ \begin{array}{l} u_i(y,t) = u_{i1}(y) + u_{i2}(y)\, e^{i\omega t} \\ \theta_i(y,t) = \theta_{i1}(y) + \theta_{i2}(y)\, e^{i\omega t} \end{array} \right\} \quad \text{for} \quad i = 1 \tag{4.1}$$

By using Equation (4.1) into the governing equations for velocity and temperature distributions and neglecting higher order terms, partial differential equations can be reduced into ordinary differential equations as follows:

4.1. Velocity Distribution

4.1.1. Steady Part

The governing equations of steady flow are:

$$\frac{d^2 u_{11}}{dy^2} - \frac{1}{S_1}\frac{d^4 u_{11}}{dy^4} - M^2 u_{11} + R_1 P_s = 0 \tag{4.2}$$

$$\frac{d^2 u_{21}}{dy^2} - \frac{1}{S_2}\frac{d^4 u_{21}}{dy^4} - M^2 \frac{\sigma'}{\mu'} u_{21} + \frac{R_2}{\rho'} P_s = 0. \tag{4.3}$$

The boundary conditions to be satisfied are:

$$\frac{d^2 u_{11}}{dy^2} = 0 \qquad \text{at } y = -1 \tag{4.4}$$

$$u_{11} = u_{11}^{'} \quad \text{at } y = -1 \tag{4.5}$$

$$\frac{du_{11}}{dy} = -\alpha\epsilon_1 (u_{11}^{'} - \frac{R_1}{\epsilon_1^2} P_s) \qquad \text{at } y = -1 \tag{4.6}$$

$$\left\{ \begin{array}{c} u_{11} = u_{21}, \ \frac{du_{11}}{dy} = \frac{du_{21}}{dy}, \ \frac{du_{11}}{dy} - \frac{1}{S_1}\frac{d^3 u_{11}}{dy^3} = \mu' \left[\frac{du_{21}}{dy} - \frac{1}{S_2}\frac{d^3 u_{21}}{dy^3} \right], \\ \frac{d^2 u_{11}}{dy2} = \eta' \frac{d^2 u_{21}}{dy2} \end{array} \right\} \text{at} \quad y = 0 \tag{4.7}$$

$$\frac{d^2 u_{21}}{dy^2} = 0 \qquad \text{at } y = 1 \tag{4.8}$$

$$u_{21} = u_{21}^{'} \quad \text{at } y = 1 \tag{4.9}$$

$$\frac{du_{21}}{dy} = \alpha\epsilon_2 (u_{21}^{'} - \frac{R_2}{\rho'\epsilon_2^2} P_s) \qquad \text{at } y = -1. \tag{4.10}$$

4.1.2. Oscillatory Part

The governing equations of oscillatory flow are:

$$\frac{d^2u_{12}}{dy^2} - \frac{1}{S_1}\frac{d^4u_{12}}{dy^4} - \left(M^2 + i\omega R_1\right)u_{12} + R_1P_o = 0 \tag{4.11}$$

$$\frac{d^2u_{22}}{dy^2} - \frac{1}{S_2}\frac{d^4u_{22}}{dy^4} - \left(M^2\frac{\sigma'}{\mu'} + i\omega R_2\right)u_{22} + \frac{R_2}{\rho'}P_o = 0. \tag{4.12}$$

The boundary conditions to be satisfied are:

$$\frac{d^2u_{12}}{dy^2} = 0 \qquad \text{at } y = -1 \tag{4.13}$$

$$u_{12} = u_{12}^{'} \qquad \text{at } y = -1 \tag{4.14}$$

$$\frac{du_{12}}{dy} = \alpha\epsilon_1(u_{12}^{'} - \frac{R_1}{\epsilon_1^2}P_o) \qquad \text{at } y = -1 \tag{4.15}$$

(4.16)
$$\left\{ \begin{array}{c} u_{12} = u_{22},\ \frac{du_{12}}{dy} = \frac{du_{22}}{dy},\ \frac{du_{12}}{dy} - \frac{1}{S_1}\frac{d^3u_{12}}{dy^3} = \mu'\left[\frac{du_{22}}{dy} - \frac{1}{S_2}\frac{d^3u_{22}}{dy^3}\right], \\ \frac{d^2u_{12}}{dy2} = \eta'\frac{d^2u_{22}}{dy2} \end{array} \right\} \text{at } \ y = 0$$

$$\frac{d^2u_{22}}{dy^2} = 0 \qquad \text{at } y = 1 \tag{4.17}$$

$$u_{22} = u_{22}^{'} \qquad \text{at } y = 1 \tag{4.18}$$

$$\frac{du_{22}}{dy} = -\alpha\epsilon_2(u_{22}^{'} - \frac{R_2}{\rho'\epsilon_2^2}P_o) \qquad \text{at } y = 1. \tag{4.19}$$

4.2. Temperature Distribution

4.2.1. Steady Part

The governing equations for steady flow are:

$$\frac{d^2\theta_{11}}{dy^2} + PrEc\left(\frac{du_{11}}{dy}\right)^2 + \frac{PrEc}{S_1}\left(\frac{d^2u_{11}}{dy^2}\right)^2 = 0 \tag{4.20}$$

$$\frac{k^{'}}{\mu'}\frac{d^2\theta_{21}}{dy^2} + PrEc\left(\frac{du_{21}}{dy}\right)^2 + \frac{PrEc}{S_2}\left(\frac{d^2u_{21}}{dy^2}\right)^2 = 0. \tag{4.21}$$

The boundary conditions to be satisfied are:

$$\theta_{11} = 0 \quad \text{at } \ y = -1 \tag{4.22}$$

$$\theta_{11} = \theta_{21}, \quad \frac{\partial \theta_{11}}{\partial y} = k' \frac{\partial \theta_{21}}{\partial y} \qquad \text{at } y = 0 \tag{4.23}$$

$$\theta_{21} = 1 \quad \text{at} \quad y = 1. \tag{4.24}$$

4.2.2. Oscillatory Part

The governing equations for steady flow are:

$$\frac{d^2\theta_{12}}{dy^2} + 2PrEc\frac{du_{11}}{dy}\frac{du_{12}}{dy} + \frac{2PrEc}{S_1}\frac{d^2u_{11}}{dy^2}\frac{d^2u_{12}}{dy^2} - i\omega\theta_{12} = 0 \tag{4.25}$$

$$\frac{k'}{\mu'}\frac{d^2\theta_{22}}{dy^2} + 2PrEc\frac{du_{21}}{dy}\frac{du_{22}}{dy} + \frac{2PrEc}{S_2}\frac{d^2u_{21}}{dy^2}\frac{d^2u_{22}}{dy^2} - i\omega\theta_{22} = 0. \tag{4.26}$$

The boundary conditions to be satisfied are:

$$\theta_{12} = 0 \quad \text{at} \quad y = -1 \tag{4.27}$$

$$\theta_{12} = \theta_{22}, \quad \frac{\partial \theta_{12}}{\partial y} = k' \frac{\partial \theta_{22}}{\partial y} \qquad \text{at } y = 0 \tag{4.28}$$

$$\theta_{22} = 0 \quad \text{at} \quad y = 1. \tag{4.29}$$

4.3. Velocity Profile

4.3.1. Steady Flow Solution

The solution for the steady flow described in Section 4.1.1 is given by:

$$u_{11}[y] = C_1 e^{-A_1 y} + C_2 e^{A_1 y} + C_3 e^{-A_2 y} + C_4 e^{A_2 y} + \frac{P_s R_1}{M^2} \tag{4.30}$$

$$u_{21}[y] = C_5 e^{-A_3 y} + C_6 e^{A_3 y} + C_7 e^{-A_4 y} + C_8 e^{A_4 y} + \frac{P_s R_2 \mu'}{M^2 \rho' \sigma'}, \tag{4.31}$$

where constants A_i, $i = 1, 2, 3, 4$ are provided in the appendix, whereas constants C_i, $i = 1, 2, 3, 4, 5, 6, 7, 8$ are not reported to achieve brevity.

4.3.2. Oscillatory Flow Solution

The solution for the oscillatory flow described in Section 4.1.2 is given by:

$$u_{12}[y] = C_9 e^{-A_5 y} + C_{10} e^{A_5 y} + C_{11} e^{-A_6 y} + C_{12} e^{A_6 y} + \frac{P_o R_1 S_1}{(M^2 S_1 + i\omega R_1 S_1)} \tag{4.32}$$

(4.33)
$$u_{22}[y] = C_{13}e^{-A_7 y} + C_{14}e^{A_7 y} + C_{15}e^{-A_8 y} + C_{16}e^{A_8 y} + \frac{P_o R_2 S_2 \mu'}{\rho'(M^2 S_2 \sigma' + i\omega R_2 S_2 \mu')},$$

where constants A_i, $i = 5, 6, 7, 8$ are provided in the appendix, whereas constants C_i, $i = 9, 10, 11, 12, 13, 14, 15, 16$ are not reported to achieve brevity.

4.3.3. Pulsatile Flow Solution

The solution for the pulsatile velocity profile is given by:

(4.34)
$$\begin{aligned} u_1[y,t] &= u_{11}[y] + u_{12}[y]e^{i\omega t} \\ u_2[y,t] &= u_{21}[y] + u_{22}[y]e^{i\omega t}, \end{aligned}$$

where $u_{11}[y], u_{12}[y], u_{21}[y]$, and $u_{22}[y]$ are known from the Equations (4.30), (4.31), (4.32), and (4.33), respectively.

4.4. Temperature Profile

4.4.1. Steady Flow Solution

The solution for the steady flow described in Section 4.2.1 is given by:

(4.35)
$$\begin{aligned} \theta_{11}[y] = {} & C_{17} + C_{18}y \\ & - \frac{EcPr}{4S_1}\Big[N_1 e^{-2A_1 y} + N_2 e^{2A_1 y} + N_3 y^2 + M_9 e^{-2A_2 y} + M_{10} e^{2A_2 y} \\ & + 8A_1 A_2 e^{-(A_1+A_2)y}\left\{M_{11}e^{2A_1 y} + M_{12} + C_4 e^{2A_2 y}\left\{M_{13} + M_{14}e^{2A_1 y}\right\}\right\}\Big] \end{aligned}$$

(4.36)
$$\begin{aligned} \theta_{21}[y] = {} & C_{19} + C_{20}y \\ & - \frac{EcPr\mu'}{4S_2 k'}\Big[N_4 e^{-2A_3 y} + N_5 e^{2A_3 y} + N_6 y^2 + M_{23} e^{-2A_4 y} + M_{24} e^{2A_4 y} \\ & + 8A_3 A_4 e^{-(A_3+A_4)y}\left\{M_{25}e^{2A_3 y} + M_{26} + C_8 e^{2A_4 y}\left\{M_{27} + M_{28}e^{2A_1 y}\right\}\right\}\Big], \end{aligned}$$

where constants A_i, $i = 5, 6, 7, 8$ are provided in the appendix, whereas constants C_i, $i = 9, 10, 11, 12, 13, 14, 15, 16$ are not reported to achieve brevity.

4.4.2. Oscillatory Flow Solution

The solution for the oscillatory flow described in Section 4.2.2 is given by:

(4.37)
$$\begin{aligned}\theta_{21}[y] = {} & C_{21}e^{\sqrt{i\omega}y} + C_{22}e^{-\sqrt{i\omega}y} \\ & + 2PrEc\Big[N_7e^{l_5y} + N_8e^{l_6y} + N_9e^{l_7y} + N_{10}e^{l_8y} + N_{11}e^{l_9y} \\ & + N_{12}e^{l_{10}y} + N_{13}e^{l_{11}y} + N_{14}e^{l_{12}y} + N_{15}e^{l_{13}y} + N_{16}e^{l_{14}y} \\ & + N_{17}e^{l_{15}y} + N_{18}e^{l_{16}y} + N_{19}e^{l_{17}y} + N_{20}e^{l_{18}y} + N_{21}e^{l_{19}y} + N_{22}e^{l_{20}y}\Big]\end{aligned}$$

(4.38)
$$\begin{aligned}\theta_{22}[y] = {} & C_{23}e^{\sqrt{\frac{i\omega\mu'}{k'}}y} + C_{24}e^{\sqrt{\frac{i\omega\mu'}{k'}}y} \\ & + 2PrEc\Big[N_{23}e^{l_{21}y} + N_{24}e^{l_{22}y} + N_{25}e^{l_{23}y} + N_{26}e^{l_{24}y} + N_{27}e^{l_{25}y} \\ & + N_{28}e^{l_{26}y} + N_{29}e^{l_{27}y} + N_{30}e^{l_{28}y} + N_{31}e^{l_{29}y} + N_{32}e^{l_{30}y} \\ & + N_{33}e^{l_{31}y} + N_{34}e^{l_{32}y} + N_{35}e^{l_{33}y} + N_{36}e^{l_{34}y} + N_{37}e^{l_{35}y} + N_{38}e^{l_{36}y}\Big],\end{aligned}$$

where constants C_i, $i = 17$ to 24 are not reported to achieve brevity, and all N_i's and M_i's are provided in the appendix.

4.4.3. Pulsatile Flow Solution

The solution for the pulsatile temperature profile is given by:

(4.39)
$$\begin{aligned}\theta_1[y,t] &= \theta_{11}[y] + \theta_{12}[y]e^{i\omega t} \\ \theta_2[y,t] &= \theta_{21}[y] + \theta_{22}[y]e^{i\omega t},\end{aligned}$$

where $\theta_{11}[y]$, $\theta_{12}[y]$, $\theta_{21}[y]$ and $\theta_{22}[y]$ are known from Equations (4.35), (4.36), (4.37), and (4.38), respectively.

4.5. Mass Flux

The instantaneous mass fluxes are given by:

$$\begin{aligned}Q_1 &= \int_{-1}^{0} u_{11}dy + \left[\int_{-1}^{0} u_{12}dy\right]e^{i\omega t} \\ Q_2 &= \int_{0}^{1} u_{21}dy + \left[\int_{0}^{1} u_{22}dy\right]e^{i\omega t},\end{aligned}$$

where Q_1 and Q_2 are mass fluxes, respectively, in Regions I and II.

4.6. Shear Stress

The shear stress in non dimensional forms at the permeable beds are given by:

$$\tau_1 = \frac{\partial u_1}{\partial y} \qquad \text{at } y = -1 \tag{4.40}$$

$$\tau_2 = \frac{\partial u_2}{\partial y} \qquad \text{at } y = 1. \tag{4.41}$$

4.7. Rate of Heat Transfer

The rates of heat transfer through the permeable beds to the fluid in the non dimensional form are given by:

$$RT_1 = \frac{\partial \theta_1}{\partial y} \qquad \text{at } y = -1 \tag{4.42}$$

$$RT_2 = \frac{\partial \theta_2}{\partial y} \qquad \text{at } y = 1. \tag{4.43}$$

5. Results and Discussion

In Section 4, we present analytical solutions for not only the pulsating velocity, temperature profile, and mass flux but also shear stress and heat flux at both permeable beds. The analytical expressions were evaluated numerically for different flow parameters values. The results are depicted graphically in Figs. 2–8 and numerically in tables. In the numerical evaluation, we take $R_2 = \frac{\rho'}{\mu'} R_1$, $S_2 = \frac{\mu'}{\eta'} S_1$, and $\epsilon_1 = \epsilon_2 = \epsilon$.

Figure 2 shows the pulsating velocity (Figs. 2a and 2b) and temperature (Figs. 2c and 2d) profiles in both regions. The velocity corresponds to slip velocities at the interfaces of the lower ($y = -1$) and upper permeable beds ($y = 1$). With one parameter kept fixed, Figs. 3a and 3b depict the variation in flow velocity with respect to couple stress parameter S_1 and Hartmann number M. At $M = 0.4$ and above, with an increase in S_1, flow velocity in both the regions decreased, whereas at $M = 0.3$, flow velocity increased with an increase in S_1. Temperature profiles with respect to S_1 and M are presented in Figs. 3c and 3d. An increment in M or a decrement in S_1 resulted in an increment in temperature in both the regions. This was attributed to the fact that as S_1 decreases, couple stress velocity increases, which in turn enhances the internal heat. The temperature increases with an increase in M, and the increment in temperature occurs due to the Joule heating effect. Velocity and temperature profiles with respect to the slip parameter α and porosity parameter ϵ are presented in Fig. 4. The velocity in both the regions increased with an increase in α or a decrease in ϵ (Figs. 4a and 4b). The temperature in both the regions increased with an increase in α or a decrease in ϵ

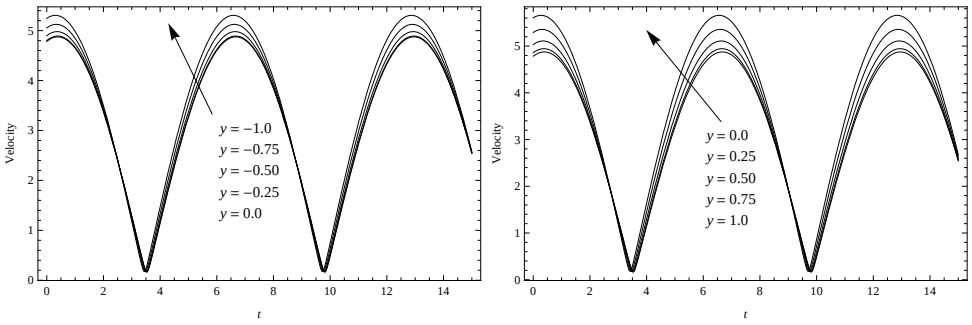

(a) Velocity profile in Region I (b) Velocity profile in Region II

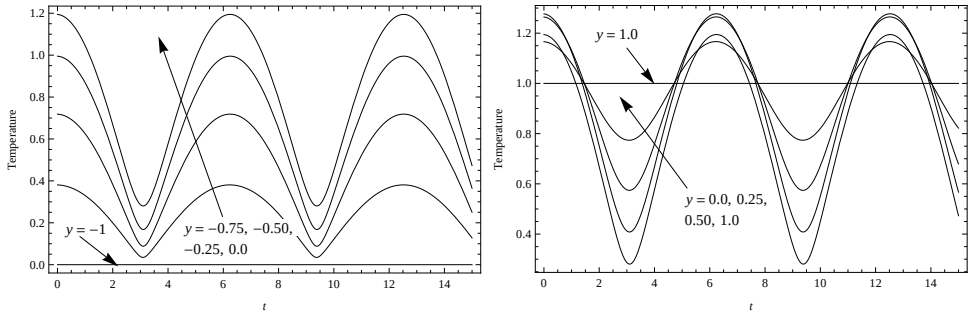

(c) Temperature profile in Region I (d) Temperature profile in Region II

Figure 2: Velocity and temperature profiles with time t at $\rho' = 0.6, \mu' = 0.8, R_1 = 1, S_1 = 1, k' = 1.2, M = 1, \sigma' = 1.2, Pr = 1, Ec = 1, \eta' = 0.8, \epsilon = 0.5, \alpha = 0.6, P_s = 1, P_o = 1, \omega = 1$.

(Figs. 4c and 4d). At $\epsilon = 1$, the temperature profile was linear (Fig. 4d), whereas the variation in α appeared to exert no effect on the temperature. The effects of viscosity ratio coefficient μ' and couple stress viscosity ratio coefficient η' are depicted in Fig. 5. An increase in μ' or a decrease in η' resulted in a decrease in flow velocity because as μ' increases, fluids become thicker. A similar trend was noted for the temperature profile.

Figure 6 presents the variation in temperature with respect to Prandtl number Pr, Eckert number Ec, electric conductivity ratio σ', and thermal conductivity ratio k'. From Figs. 6a and 6b, it can be observed that as Pr increased, the temperature profile also increased. This increase is attributed to an increase in viscous diffusion in the presence of viscous dissipation, which enhances internal heat generation. As Ec increased, fluid frictional effects increased and hence the temperature profile increased. However, the temperature also increased with an increase in σ' (Fig. 6c), whereas it decreased with an increase in k' (Fig. 6d). From Figs. 7a and 7b, we observed that as the frequency parameter ωt increased, the

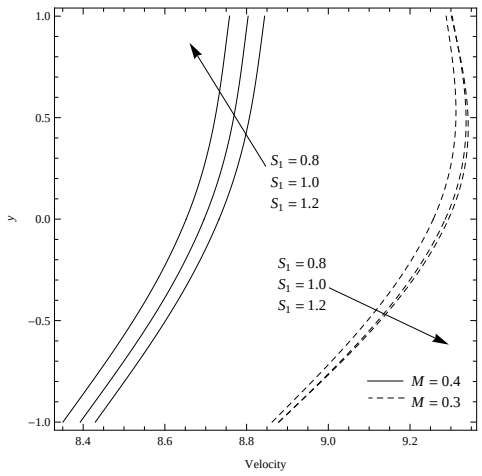

(a) Variation in velocity with S_1 at constant M

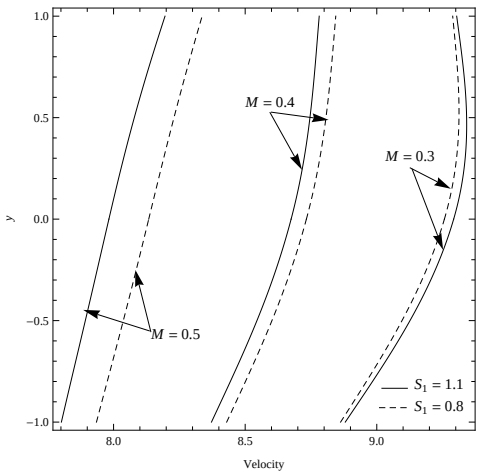

(b) Variation in velocity with M at constant S_1

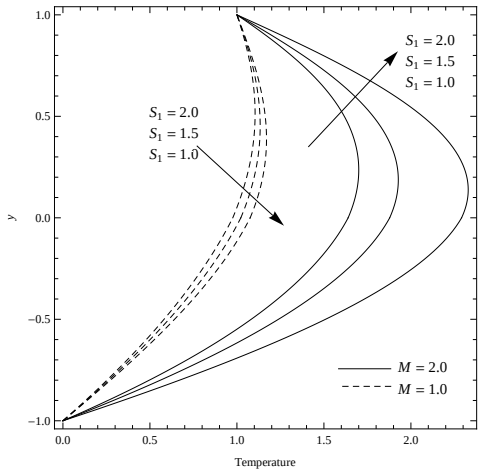

(c) Variation in temperature with S_1 at constant M

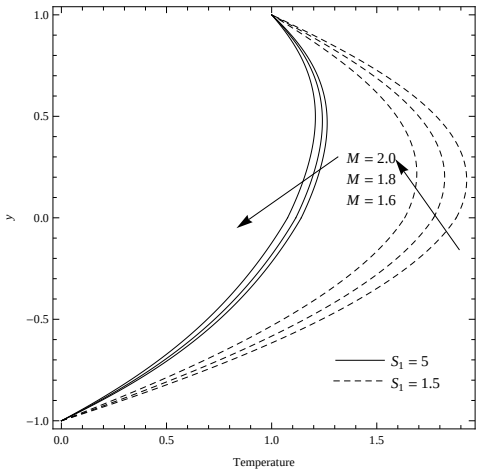

(d) Variation in temperature with M at constant S_1

Figure 3: Velocity and temperature profiles with time M and S_1 at $\rho' = 0.6, \mu' = 0.8, R_1 = 1, k' = 1.2, \sigma' = 1.2, Pr = 1, Ec = 1, \eta' = 0.8, \epsilon = 0.5, \alpha = 0.6, P_s = 1, P_o = 1, \omega t = \frac{\pi}{4}$.

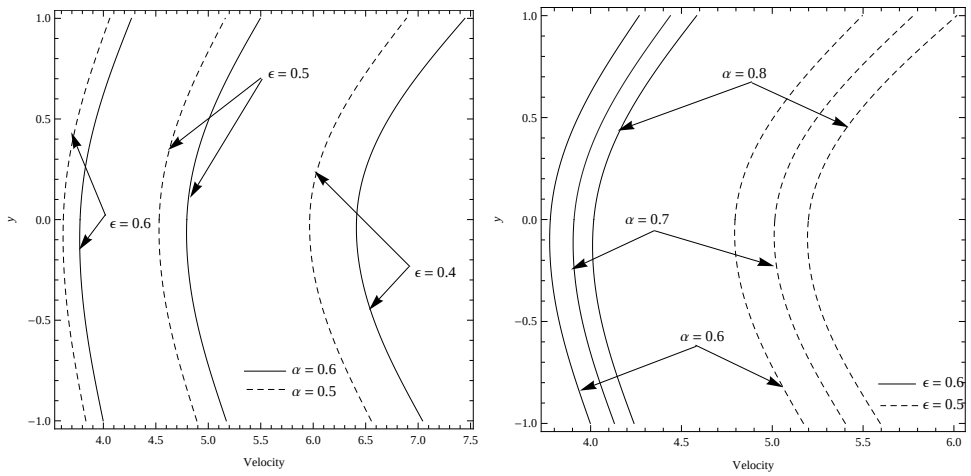

(a) Variation in velocity with ϵ at constant α

(b) Variation in velocity with α at constant ϵ

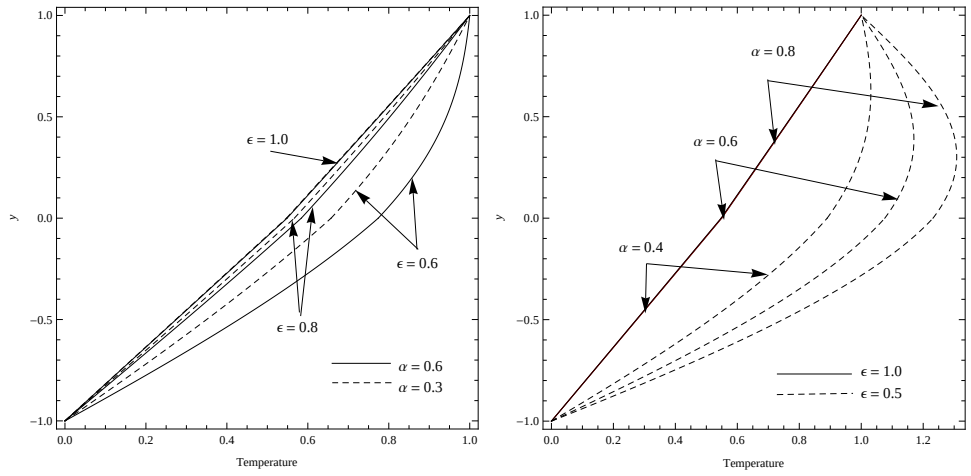

(c) Variation in temperature with ϵ at constant α

(d) Variation in temperature with α at constant ϵ

Figure 4: Velocity and temperature profiles with time α and ϵ at $\rho' = 0.6, \mu' = 0.8, R_1 = 1, S_1 = 1, k' = 1.2, M = 1, \sigma' = 1.2, Pr = 1, Ec = 1, \eta' = 0.8, P_s = 1, P_o = 1, \omega t = \frac{\pi}{4}$.

flow velocity and temperature in both the regions decreased. Figure 8 presents the variation in velocity and temperature profiles when fluids in both the regions were considered identical. Figures 8a and 8b depict the velocity and temperature profiles, respectively, when $M = 0$. The velocity profile resembles the Hagen–Poiseuille flow, and the temperature profile is almost linear. Further, the velocity at permeable beds becomes zero for $\epsilon \to \infty$ (Fig. 8c).

Non dimensional shear stresses at lower and upper permeable beds were evaluated numerically, and the results are presented in Table 1. As ωt increased, shear stress at the lower permeable bed increased, whereas at the upper permeable bed, as ωt increased through values 0 to $\frac{\pi}{4}$, shear stress decreased, and a further increase in ωt resulted in an increase in shear stress. From Table 1, it is clear that as ρ', α, R_1, and S_1 increased, shear stress at both the permeable beds also increased, whereas as μ', η', and ϵ increased, shear stress at both the permeable beds decreased. As M increased, shear stress at the lower permeable bed decreased, whereas shear stress at the upper permeable bed increased with an increase in M.

Numerical values of rates of heat transfer through both the permeable beds to the fluid were calculated for different values of governing flow parameters and are given in Table 2. As $\omega t, \epsilon$, and μ' increased, the rate of heat transfer through the lower permeable bed decreased, whereas the rate of heat transfer through the upper permeable bed increased. As $k', \eta', \alpha, R_1, Pr$, and Ec increased, rates of heat transfer through the lower and upper permeable beds increased and decreased, respectively. As σ' increased, the rate of heat transfer through the lower permeable bed decreased, whereas as σ' increased through values 0.8 to 1.0, the rate of heat transfer through the upper permeable bed increased, and a further increase in σ' resulted in a decrease in the rate of heat transfer through the upper permeable bed. As S_1 increased, the rate of heat transfer through the lower permeable bed decreased, whereas as S_1 increased through values 0.3 to 0.4, the rate of heat transfer through the upper permeable bed increased, and a further increase in S_1 resulted in a decrease in the rate of heat transfer through the upper permeable bed. The rate of heat transfer through the lower permeable bed first increased and then decreased with an increase in M, whereas the rate of heat transfer through the upper permeable bed increased with an increase in M.

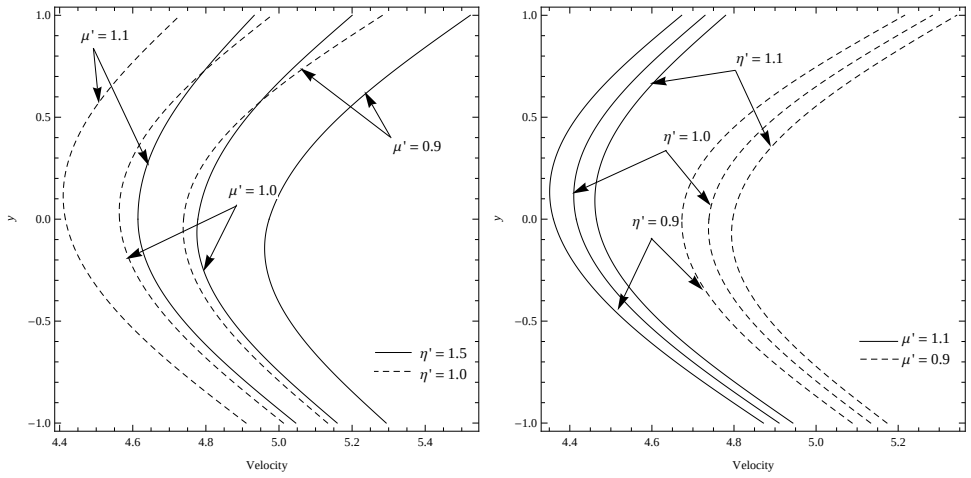

(a) Variation in velocity with μ' at constant η'

(b) Variation in velocity with η' at constant μ'

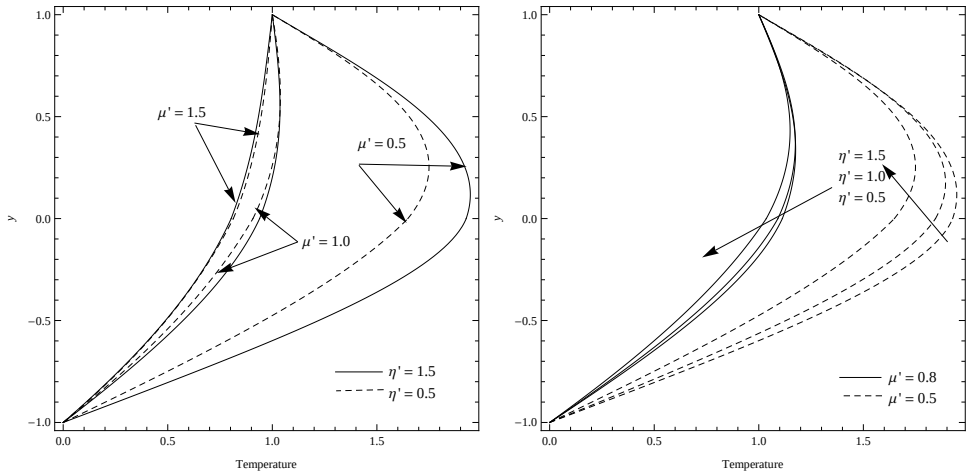

(c) Variation in temperature with μ' at constant η'

(d) Variation in temperature with η' at constant μ'

Figure 5: Velocity and temperature profiles with time μ' and η' at $\rho' = 0.6, R_1 = 1, S_1 = 1, k' = 1.2, M = 1, \sigma' = 1.2, Pr = 1, Ec = 1, \epsilon = 0.5, \alpha = 0.6, P_s = 1, P_o = 1, \omega t = \frac{\pi}{4}$.

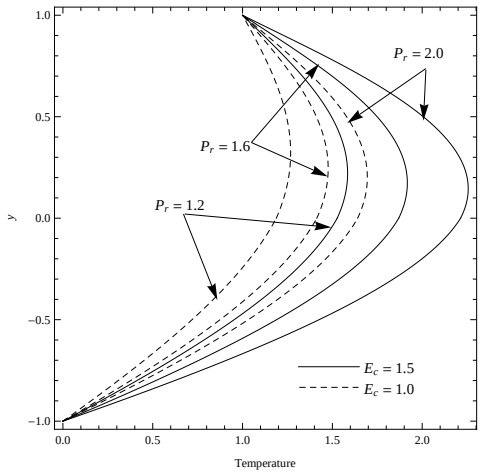

(a) Variation in temperature at $k' = 1.2, \sigma' = 1.2$

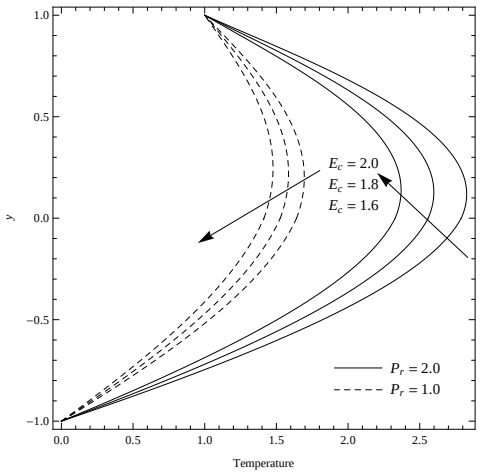

(b) Variation in temperature at $k' = 1.2, \sigma' = 1.2$

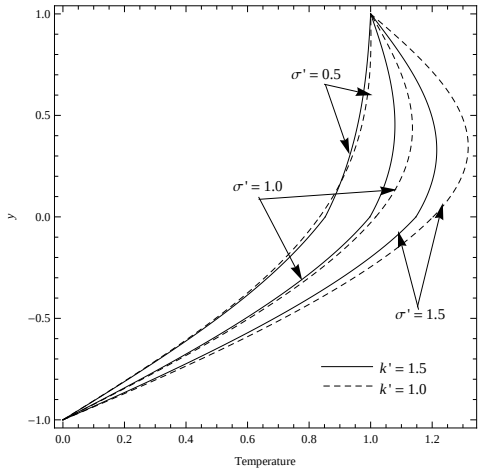

(c) Variation in temperature at $P_r = 1, E_c = 1$

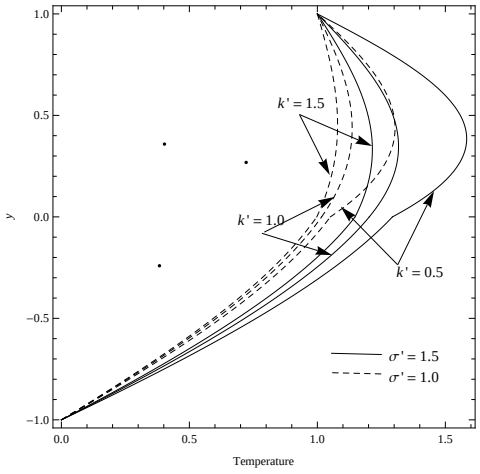

(d) Variation in temperature at $P_r = 1, E_c = 1$

Figure 6: Temperature profiles with Pr, Ec, σ' and k' at $\rho' = 0.6, \mu' = 0.8, R_1 = 1, S_1 = 1, M = 1, \eta' = 0.8, \epsilon = 0.5, \alpha = 0.6, P_s = 1, P_o = 1, \omega t = \frac{\pi}{4}$.

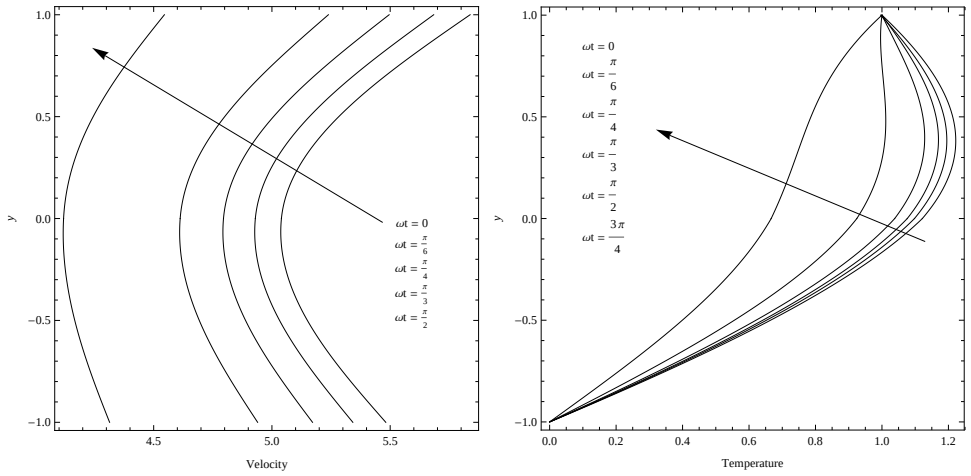

(a) Variation in velocity with ωt (b) Variation in temperature with ωt

Figure 7: Velocity and temperature profiles with ωt at $\rho' = 0.6, \mu' = 0.8, R_1 = 1, S_1 = 1, k' = 1.2, M = 1, \sigma' = 1.2, Pr = 1, Ec = 1, \eta' = 0.8, \epsilon = 0.5, \alpha = 0.6, P_s = 1, P_o = 1$.

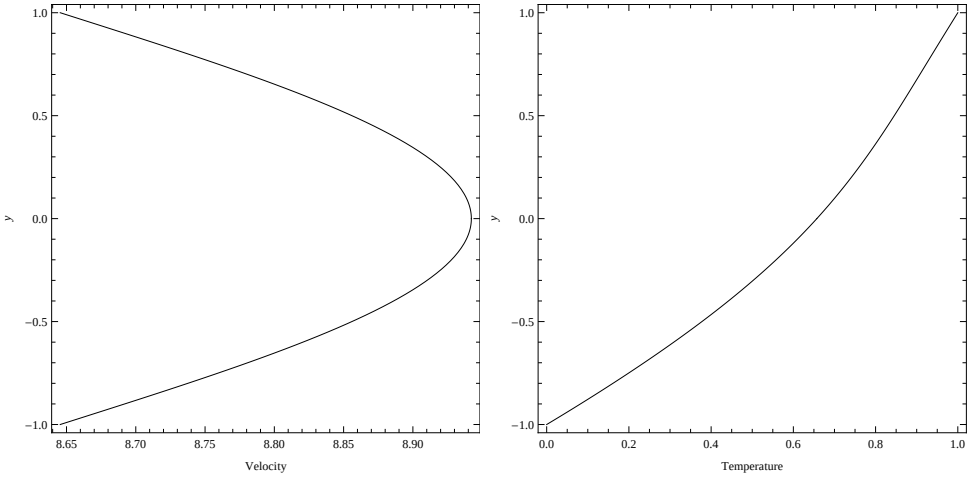

(a) Velocity profile for same fluids at $M = 0$ (b) Temperature profile for same fluids at $M = 0$

Figure 8: Some particular cases.

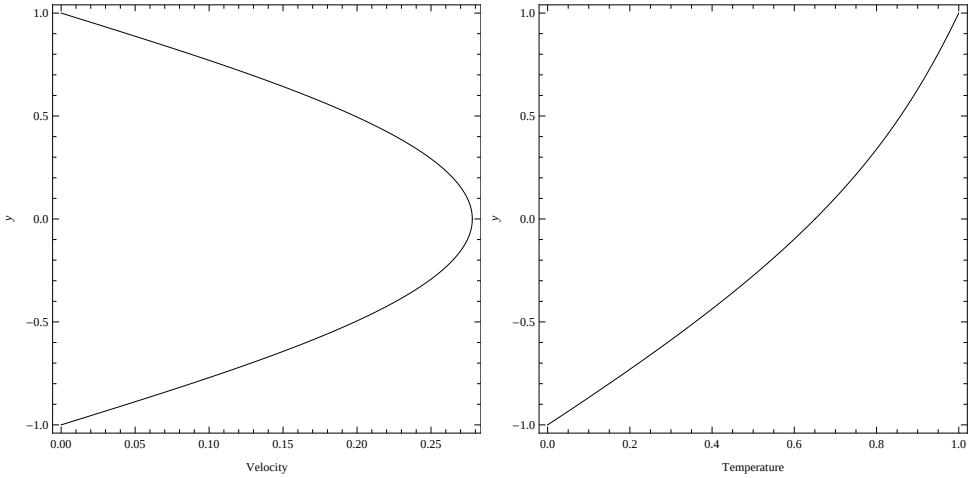

(c) Velocity profile for same fluids at $M = 0, \epsilon \to \infty$

(d) Temperature profile for same fluids at $M = 0, \epsilon \to \infty$

Figure 8: Some particular cases.(cont...)

6. Summary

We analysed the MHD pulsating flow and heat transfer of two immiscible, incompressible, and conducting couple stress fluids between two permeable beds. The analytical solutions of the velocity profile, temperature profile, mass flux, shear stress, and rate of heat transfer were obtained. Analytical solutions were numerically evaluated for the different values of governing flow parameters. The effects of the flow parameters on flow velocity and temperature variation are depicted through graphs, whereas variations in shear stress and rate of heat transfer at the permeable beds are presented through tables. The following conclusions can be drawn from the entire analysis:

- The velocity profile decreases as M increases. At $M = 0.4$ or above, velocity is a decreasing function of couple stress parameter S_1, whereas at $M = 0.3$ or below, velocity is an increasing function of S_1.
- Both velocity and temperature increase as the slip parameter α increases, whereas for porosity parameter ϵ, both exhibit an inverse behaviour.
- An increase in viscosity ratio μ' or a decrease in couple stress viscosity ratio results in a decrease in both the velocity and temperature profile.
- The temperature profile is an increasing function of Prandtl number Pr, Eckert number Ec, and electric conductivity ratio σ', whereas increases in the thermal conductivity ratio k' have the tendency to cool down the thermal state.

- When $M = 0$, the temperature profile is nearly linear.
- An increase in the density ratio ρ', slip parameter α, Reynolds number R_1, and couple stress parameter S_1, the shear stress at both the permeable beds increases. However shear stress shows a reverse trend for viscosity ratio μ', couple stress viscosity ratio η', and porosity parameter ϵ.
- The rates of heat transfer at both the permeable beds are positive for the considered set of parameters, which indicates that heat is transferred to the permeable beds by the fluids. This occurs due to internal heat generation by viscous dissipation effects.

References

[1] T. T. Ariman and N. D. Sylvester, *Microcontinum fluid mechanics–a review*, Int. J. Eng. Sci., **11(8)**(1973), 905–930.

[2] T. T. Ariman and N. D. Sylvester, *Applications of microcontinuum fluid mechanics*, Int. J. Eng. Sci., **12(4)**(1974), 273–293.

[3] G. Beavers and D. Joseph, *Boundary conditions at naturally permeable wall*, J. Fluid Mech., **30(1)**(1967), 197–207.

[4] N. M. Bujurke and G. Jayaraman, *The influence of couple stresses in squeeze films*, Int. J. Mech. Sci., **24(6)**(1982), 369–376.

[5] P. Chaturani and R. P. Samy, *A study of non-Newtonian aspects of blood flow through stenosed arteries and its applications in arterial diseases*, Biorheology, **22(6)**(1985), 521–531.

[6] A. A. Elsharkawy and L. H. Guedouar, *An inverse solution for finite journal bearings lubricated with couple stress fluids*, Tribol. Int., **34(2)**(2001), 107–108.

[7] M. Farooq et.al., *Heat transfer flow of steady couple stress fluids between two parallel plates with variable viscosity*, Heat Transfer Res., **42(8)**(2011), 737–780.

[8] A. E. Garcia and D. N. Riahi, *Two phase blood flow and heat transfer in an inclined stenosed artery with or without a catheter*, Int. J. Fluid Mech. Res., **41(1)**(2014), 16–30.

[9] R. S. Gupta and L. G. Sharma, *Analysis of couple stress lubricant in hydrostatic thrust bearings*, Wear, **125(3)**(1988), 257–270.

[10] D. P. Hochmuth and D. K. Sunada, *Ground-water model of two-phase immiscible flow in coarse material*, Groundwater, **23(5)**(1985), 617–626.

[11] S. Islam and C. Y. Zhou, *Exact solutions for two-dimensional flows of couple stress fluids*, ZAMP, **58(6)**(2007), 1035–1048.

[12] T. K. V. Iyengar and B. Punnamchandar, *Pulsating flow of an incompressible couple stress fluid between permeable beds*, Int. J. Math. Comput. Phys. Elect. Comp. Eng., **5(8)**(2011), 1241–1251.

[13] D. Jogie and B. Bhatt, *Flow of immiscible fluids in a naturally permeable channel*, Int. J. Pure Appl. Math., **78(3)**(2012), 435–449.

[14] J. R. Lin, *Static and dynamic behaviour of externally pressurized circular step thrust bearings lubricated with couple stress fluids*, Tribol. Int., **32(4)**(1999), 207–216.

[15] C. B. Mehta et.al., *Thermal convection of magneto compressible couple stress fluid saturated in a porous medium with hall current*, Int. J. Appl. Mech. Eng., **21(1)**(2016), 83–93.

[16] U. M. Mokhiamer et.al., *A study of a journal bearing lubricated by fluids with couple stress considering the elasticity of the linear*, Wear, **224(2)**(1999), 194–201.

[17] S. Panda, S. C. Martha and A. Chakrabarti, *Three-layer fluid flow over a small obstruction on the bottom of a channel*, ANZIAM J., **56(3)**(2015), 248–274.

[18] B. G. Prasad and A. Kumar, *Flow of a hydromagnetic fluid through porous media between permeable beds under exponentially decaying pressure gradient*, Comput. Meth. Sci. Technol., **17(1-2)**(2011), 63–74.

[19] B. Punnamchandar and T. K. V. Iyengar, *Oscillatory flow of an incompressible couple stress fluid between permeable beds with an imposed uniform magnetic field*, Spec. Topics Rev. Porous Media, **4(1)**(2013), 23–31.

[20] G. Ramanaiah, *Squeeze films between finite plates lubricated by fluids with couple stress*, Wear, **54(2)**(1979), 315–320.

[21] M. Sharan and A. S. Popel, *A two-phase model for flow of blood in narrow tubes with increased effective viscosity near the wall*, Biorheology, **38(5-6)**(2001), 415–428.

[22] A. M. Siddiqui et al., *Couette and Poiseuille flows for non-Newtonian fluids*, Int. J. Nonlin. Sci. Num. Sim., **7(1)**(2006), 15–26.

[23] V. M. Soundalgekar and R. N. Aranake, *Effects of couple stresses on MHD Couette flow*, Nucl. Eng. Design, **49(3)**(1978), 197–203.

[24] J. Srinivas, *Entropy generation analysis of the flow of two immiscible couple stress fluids between two porous beds*, Comput. Therm. Sci., **7(2)**(2015), 123–137.

[25] J. Srinivas and J. V. R. Murthy, *Flow of two immiscible couple stress fluids between two permeable beds*, J. Appl. Fluid Mech., **9(1)**(2016), 501–507.

[26] L. M. Srivastava, *Flow of couple stress fluid through stenotic blood vessels*, J. Bio-Mech., **18(7)**(1985), 479–485.

[27] L. M. Srivastava, *Peristaltic transport of a couple stress fluid*, Rheol. Acta, **25(6)**(1986), 638–641.

[28] V. K. Stokes, *Couple stresses in fluids*, Phys. Fluids, **9(9)**(1966), 1709–1715.

[29] V. K. Stokes, *Theories of fluids with microstructure, an introduction*, Springer Verlag, New York, 1984.

[30] A. Z. Szeri and K. R. Rajagopal, *Flow of a non-Newtonian fluid between heated parallel plates*, Int. J. of Nonlin. Mech., **20(2)**(1985), 91–101.

[31] J. C. Umavathi, I. C. Liu and J. Prathap-Kumar, *Unsteady flow and heat transfer of porous media sandwiched between viscous fluids*, Appl. Math. Mech. (Engl. Ed.), **31(12)**(2010), 1497–1516.

[32] K. Vajravelu, P. V. Arunachalam and S. Sreenadh, *Unsteady flow of two immiscible conducting fluids between two permeable beds*, J. Math. Anal. Appl., **196(3)**(1995), 1105–1116.

[33] K. Vajravelu, K. Ramesh, S. Sreenadh, and P.V. Arunachalam, *Pulsatile flow between permeable beds*, Int. J. Non-Linear Mech., **38(7)**(2003), 999–1005.

Appendix

$l_1 = \sqrt{S_1(-4M^2+S_1)}, l_2 = \frac{\sqrt{S_2\mu'(S_2\mu'-4M^2\sigma)}}{\mu'}, l_3 = \sqrt{S_1(-4M^2-4i\omega R_1+S_1)},$
$l_4 = \frac{\sqrt{S_2\mu'(-4M^2\sigma'+S_2\mu'-4i\omega R_2\mu')}}{\mu'}$, $l_5 = -A_1 - A_5$, $l_6 = A_1 - A_5$, $l_7 = -A_2 - A_5$, $l_8 = A_2 - A_5$, $l_9 = -A_1 + A_5$, $l_{10} = -A_1 + A_5$, $l_{11} = -A_2 + A_5$, $l_{12} = A_2 + A_5$, $l_{13} = -A_1 - A_6$, $l_{14} = A_1 - A_6$, $l_{15} = -A_2 - A_6$, $l_{16} = A_2 - A_6$, $l_{17} = -A_1 + A_6$, $l_{18} = A_1 + A_6$, $l_{19} = -A_2 + A_6$, $l_{20} = A_2 + A_6$, $l_{21} = -A_3 - A_7$, $l_{22} = A_3 - A_7$, $l_{23} = -A_4 - A_7$, $l_{24} = A_4 - A_7$, $l_{25} = -A_3 + A_7$, $l_{26} = -A_3 + A_7$, $l_{27} = -A_4 + A_7$, $l_{28} = A_4 + A_7$, $l_{29} = -A_3 - A_8$, $l_{30} = A_3 - A_8$, $l_{31} = -A_4 - A_8$, $l_{32} = A_4 - A_8$, $l_{33} = -A_3 + A_8$, $l_{34} = A_3 + A_8$, $l_{35} = -A_4 + A_8$, $l_{36} = A_4 + A_8$

$A_1 = \sqrt{\frac{S_1-l_1}{2}}$, $A_2 = \sqrt{\frac{S_1+l_1}{2}}$, $A_3 = \sqrt{\frac{S_2-l_2}{2}}$, $A_4 = \sqrt{\frac{S_2+l_2}{2}}$ $A_5 = \sqrt{\frac{S_1-l_3}{2}}$, $A_6 = \sqrt{\frac{S_1+l_3}{2}}$, $A_7 = \sqrt{\frac{S_2-l_4}{2}}$, $A_8 = \sqrt{\frac{S_2+l_4}{2}}$

$M_1 = C_1^2A_1^2$, $M_2 = C_2^2A_1^2$, $M_3 = 4C_1C_2A_1^4$,$M_4 = 4C_3C_4A_2^4$, $M_5 = C_1^2S_1$, $M_6 = C_2^2S_1$, $M_7 = 4C_1C_2A_1^2S_1$, $M_8 = 4C_3C_4A_2^2S_1$, $M_9 = C_3^2(A_2^2+S_1)$, $M_{10} = C_4^2(A_2^2+S_1)$, $M_{11} = \frac{C_2C_3(A_1A_2-S_1)}{(A_1-A_2)^2}$, $M_{12} = \frac{C_1C_3(A_1A_2+S_1)}{(A_1+A_2)^2}$, $M_{13} = \frac{C_1(A_1A_2-S_1)}{(A_1-A_2)^2}$, $M_{14} = \frac{C_2(A_1A_2+S_1)}{(A_1+A_2)^2}$, $M_{15} = C_5^2A_3^2$, $M_{16} = C_6^2A_3^2$, $M_{17} = 4C_5C_6A_3^4$, $M_{18} = 4C_7C_8A_4^4$ $M_{19} = C_5^2S_2$, $M_{20} = C_6^2S_2$, $M_{21} = 4C_5C_6A_3^2S_2$, $M_{22} = 4C_7C_8A_4^2S_2$, $M_{23} = C_7^2(A_4^2+S_2)$, $M_{24} = C_8^2(A_4^2+S_2)$, $M_{25} = \frac{C_6C_7(A_3A_4-S_2)}{(A_3-A_4)^2}$, $M_{26} = \frac{C_6C_7(A_3A_4+S_2)}{(A_3+A_4)^2}$, $M_{27} = \frac{C_5(A_3A_4-S_2)}{(A_3-A_4)^2}$, $M_{28} = \frac{C_6(A_3A_4+S_2)}{(A_3+A_4)^2}$ $M_{29} = A_1A_5C_1C_9$, $M_{30} = -A_1A_5C_2C_9$, $M_{31} = A_2A_5C_3C_9$, $M_{32} = -A_2A_5C_4C_9$, $M_{33} = -A_1A_5C_1C_{10}$, $M_{34} = A_1A_5C_2C_{10}$, $M_{35} = -A_2A_5C_3C_{10}$, $M_{36} = A_2A_5C_4C_{10}$, $M_{37} = A_1A_6C_1C_{11}$, $M_{38} = -A_1A_6C_2C_{11}$, $M_{39} = A_2A_6C_3C_{11}$, $M_{40} = -A_2A_6C_4C_{11}$, $M_{41} = -A_1A_6C_1C_{12}$, $M_{42} = A_1A_6C_2C_{11}$, $M_{43} = -A_2A_6C_3C_{12}$, $M_{44} = A_2A_6C_4C_{12}$, $M_{45} = A_1^2A_5^2C_1C_9$, $M_{46} = A_1^2A_5^2C_2C_9$, $M_{47} = A_2^2A_5^2C_3C_9$, $M_{48} = A_2^2A_5^2C_4C_9$, $M_{49} = A_1^2A_5^2C_1C_{10}$, $M_{50} = A_1^2A_5^2C_2C_{10}$, $M_{51} = A_2^2A_5^2C_3C_{10}$, $M_{52} = A_2^2A_5^2C_4C_{10}$, $M_{53} = A_1^2A_6^2C_1C_{11}$, $M_{54} = A_1^2A_6^2C_2C_{11}$, $M_{55} = A_2^2A_6^2C_3C_{11}$, $M_{56} = A_2^2A_6^2C_4C_{11}$, $M_{57} = A_1^2A_6^2C_1C_{12}$, $M_{58} = A_1^2A_6^2C_2C_{11}$, $M_{59} = A_2^2A_6^2C_3C_{12}$, $M_{60} = A_2^2A_6^2C_4C_{12}$, $M_{61} = A_3A_7C_5C_{13}$, $M_{62} = -A_3A_7C_6C_{13}$, $M_{63} = A_4A_7C_7C_{13}$, $M_{64} = -A_4A_7C_8C_{13}$, $M_{65} = -A_3A_7C_5C_{14}$, $M_{66} = A_3A_7C_6C_{14}$, $M_{67} = -A_4A_7C_7C_{14}$, $M_{68} = A_4A_7C_8C_{14}$, $M_{69} = A_3A_8C_5C_{15}$, $M_{70} = -A_3A_8C_6C_{15}$, $M_{71} = A_4A_8C_7C_{15}$, $M_{72} = -A_4A_8C_8C_{15}$, $M_{73} = -A_3A_8C_5C_{16}$, $M_{74} = A_3A_8C_6C_{15}$, $M_{75} = -A_4A_8C_7C_{16}$, $M_{76} = A_4A_8C_8C_{16}$, $M_{77} = A_3^2A_7^2C_5C_{13}$, $M_{78} = A_3^2A_7^2C_6C_{13}$, $M_{79} = A_4^2A_7^2C_7C_{13}$, $M_{80} = A_4^2A_7^2C_8C_{13}$, $M_{81} = A_3^2A_7^2C_5C_{14}$, $M_{82} = A_3^2A_7^2C_6C_{14}$, $M_{83} = A_4^2A_7^2C_7C_{14}$, $M_{84} = A_4^2A_7^2C_8C_{14}$, $M_{85} = A_3^2A_8^2C_5C_{15}$, $M_{86} = A_3^2A_8^2C_6C_{15}$, $M_{87} = A_4^2A_8^2C_7C_{15}$, $M_{88} = A_4^2A_8^2C_8C_{15}$, $M_{89} = A_3^2A_8^2C_5C_{16}$, $M_{90} = A_3^2A_8^2C_6C_{15}$, $M_{91} = A_4^2A_8^2C_7C_{16}$, $M_{92} = A_4^2A_8^2C_8C_{16}$,

$N_1 = M_1 + M_5$, $N_2 = M_2 + M_6$, $N_3 = M_3 + M_4 - M_7 - M_8$, $N_4 = M_{15} + M_{19}$, $N_5 = M_{16} + M_{20}$, $N_6 = M_{17} + M_{18} - M_{21} - M_{22}$

$N_7 = \frac{1}{l_5^2-i\omega}[M_{29} + \frac{1}{S_1}M_{45}]$, $N_8 = \frac{1}{l_6^2-i\omega}[M_{30} + \frac{1}{S_1}M_{46}]$, $N_9 = \frac{1}{l_7^2-i\omega}[M_{31} + \frac{1}{S_1}M_{47}]$, $N_{10} = \frac{1}{l_8^2-i\omega}[M_{32} + \frac{1}{S_1}M_{48}]$, $N_{11} = \frac{1}{l_9^2-i\omega}[M_{33} + \frac{1}{S_1}M_{49}]$, $N_{12} = \frac{1}{l_{10}^2-i\omega}[M_{34} + \frac{1}{S_1}M_{50}]$, $N_{13} = \frac{1}{l_{11}^2-i\omega}[M_{35} + \frac{1}{S_1}M_{51}]$, $N_{14} = \frac{1}{l_{12}^2-i\omega}[M_{36} + \frac{1}{S_1}M_{52}]$, $N_{15} = \frac{1}{l_{13}^2-i\omega}[M_{37} + \frac{1}{S_1}M_{53}]$, $N_{16} = \frac{1}{l_{14}^2-i\omega}[M_{38} + \frac{1}{S_1}M_{54}]$, $N_{17} = \frac{1}{l_{15}^2-i\omega}[M_{39} + \frac{1}{S_1}M_{55}]$, $N_{18} = \frac{1}{l_{16}^2-i\omega}[M_{40} + \frac{1}{S_1}M_{56}]$, $N_{19} = \frac{1}{l_{17}^2-i\omega}[M_{41} + \frac{1}{S_1}M_{57}]$, $N_{20} = \frac{1}{l_{18}^2-i\omega}[M_{42} + \frac{1}{S_1}M_{58}]$, $N_{21} = \frac{1}{l_{19}^2-i\omega}[M_{43} + \frac{1}{S_1}M_{59}]$, $N_{22} = \frac{1}{l_{20}^2-i\omega}[M_{44} + \frac{1}{S_1}M_{60}]$, $N_{23} = \frac{1}{k'\mu' l_{21}^2-i\omega}[M_{61} + \frac{1}{S_2}M_{77}]$, $N_{24} = \frac{1}{k'\mu' l_{22}^2-i\omega}[M_{62} + \frac{1}{S_2}M_{78}]$, $N_{25} = \frac{1}{k'\mu' l_{23}^2-i\omega}[M_{63} + \frac{1}{S_2}M_{79}]$, $N_{26} = \frac{1}{k'\mu' l_{24}^2-i\omega}[M_{64} + \frac{1}{S_2}M_{80}]$, $N_{27} = \frac{1}{k'\mu' l_{25}^2-i\omega}[M_{65} + \frac{1}{S_2}M_{81}]$, $N_{28} = \frac{1}{k'\mu' l_{26}^2-i\omega}[M_{66} + \frac{1}{S_2}M_{82}]$, $N_{29} = \frac{1}{k'\mu' l_{27}^2-i\omega}[M_{67} + \frac{1}{S_2}M_{83}]$, $N_{30} = \frac{1}{k'\mu' l_{28}^2-i\omega}[M_{68} + \frac{1}{S_2}M_{84}]$, $N_{31} = \frac{1}{k'\mu' l_{29}^2-i\omega}[M_{69} + \frac{1}{S_2}M_{85}]$, $N_{32} = \frac{1}{k'\mu' l_{30}^2-i\omega}[M_{70} + \frac{1}{S_2}M_{86}]$, $N_{33} = \frac{1}{k'\mu' l_{31}^2-i\omega}[M_{71} + \frac{1}{S_2}M_{87}]$, $N_{34} = \frac{1}{k'\mu' l_{32}^2-i\omega}[M_{72} + \frac{1}{S_2}M_{88}]$, $N_{35} = \frac{1}{k'\mu' l_{33}^2-i\omega}[M_{73} + \frac{1}{S_2}M_{89}]$, $N_{36} = \frac{1}{k'\mu' l_{34}^2-i\omega}[M_{74} + \frac{1}{S_2}M_{90}]$, $N_{37} = \frac{1}{k'\mu' l_{35}^2-i\omega}[M_{75} + \frac{1}{S_2}M_{91}]$, $N_{38} = \frac{1}{k'\mu' l_{36}^2-i\omega}[M_{76} + \frac{1}{S_2}M_{92}]$,

Table 1: Non dimensional shear stress $|\tau|$ on the permeable beds.

Flow parameters														Shear stress	
ωt	ρ'	μ'	k'	σ'	η'	α	ϵ	R_1	S_1	Pr	Ec	M	P_s	P_o	LPB	UPB
$\frac{\pi}{4}$	0.6	0.8	1.2	1.2	0.9	0.5	0.5	0.5	0.5	1	1	0.5	1	1	0.116021	0.132382
0	0.6	0.8	1.2	1.2	0.9	0.5	0.5	0.5	0.5	1	1	0.5	1	1	0.068791	0.132505
$\frac{\pi}{2}$	0.6	0.8	1.2	1.2	0.9	0.5	0.5	0.5	0.5	1	1	0.5	1	1	0.187640	0.146323
$\frac{\pi}{4}$	**0.7**	0.8	1.2	1.2	0.9	0.5	0.5	0.5	0.5	1	1	0.5	1	1	0.119782	0.135635
$\frac{\pi}{4}$	**0.8**	0.8	1.2	1.2	0.9	0.5	0.5	0.5	0.5	1	1	0.5	1	1	0.123550	0.139106
$\frac{\pi}{4}$	0.6	**0.9**	1.2	1.2	0.9	0.5	0.5	0.5	0.5	1	1	0.5	1	1	0.087114	0.088189
$\frac{\pi}{4}$	0.6	**1.0**	1.2	1.2	0.9	0.5	0.5	0.5	0.5	1	1	0.5	1	1	0.073732	0.072907
$\frac{\pi}{4}$	0.6	0.8	1.2	1.2	**1.0**	0.5	0.5	0.5	0.5	1	1	0.5	1	1	0.115055	0.129550
$\frac{\pi}{4}$	0.6	0.8	1.2	1.2	**1.1**	0.5	0.5	0.5	0.5	1	1	0.5	1	1	0.114259	0.127192
$\frac{\pi}{4}$	0.6	0.8	1.2	1.2	0.9	**0.4**	0.5	0.5	0.5	1	1	0.5	1	1	0.101972	0.119945
$\frac{\pi}{4}$	0.6	0.8	1.2	1.2	0.9	**0.3**	0.5	0.5	0.5	1	1	0.5	1	1	0.086560	0.106130
$\frac{\pi}{4}$	0.6	0.8	1.2	1.2	0.9	0.5	**0.4**	0.5	0.5	1	1	0.5	1	1	0.122387	0.236372
$\frac{\pi}{4}$	0.6	0.8	1.2	1.2	0.9	0.5	**0.3**	0.5	0.5	1	1	0.5	1	1	0.192609	0.442591
$\frac{\pi}{4}$	0.6	0.8	1.2	1.2	0.9	0.5	0.5	**0.4**	0.5	1	1	0.5	1	1	0.083091	0.099219
$\frac{\pi}{4}$	0.6	0.8	1.2	1.2	0.9	0.5	0.5	**0.3**	0.5	1	1	0.5	1	1	0.055268	0.071074
$\frac{\pi}{4}$	0.6	0.8	1.2	1.2	0.9	0.5	0.5	0.5	**0.4**	1	1	0.5	1	1	0.110388	0.122198
$\frac{\pi}{4}$	0.6	0.8	1.2	1.2	0.9	0.5	0.5	0.5	**0.3**	1	1	0.5	1	1	0.104753	0.111904
$\frac{\pi}{4}$	0.6	0.8	1.2	1.2	0.9	0.5	0.5	0.5	0.5	1	1	**0.4**	1	1	0.163950	0.104179
$\frac{\pi}{4}$	0.6	0.8	1.2	1.2	0.9	0.5	0.5	0.5	0.5	1	1	**0.3**	1	1	0.208152	0.100611

Table 2: Non dimensional rate of heat transfer through the permeable beds to the fluid.

Flow parameters													Rate of heat transfer	
ωt	ρ'	μ'	k'	σ'	η'	α	ϵ	R_1	S_1	Pr	Ec	M	P_s	P_o	LPB	UPB
$\frac{\pi}{4}$	0.6	0.8	1.2	1.2	0.9	0.5	0.5	0.5	0.5	1	1	0.5	1	1	0.550676	0.450857
0	0.6	0.8	1.2	1.2	0.9	0.5	0.5	0.5	0.5	1	1	0.5	1	1	0.551730	0.446073
$\frac{\pi}{\mathbf{2}}$	0.6	0.8	1.2	1.2	0.9	0.5	0.5	0.5	0.5	1	1	0.5	1	1	0.547662	0.462045
$\frac{\pi}{4}$	0.6	**0.9**	1.2	1.2	0.9	0.5	0.5	0.5	0.5	1	1	0.5	1	1	0.546239	0.454490
$\frac{\pi}{4}$	0.6	**1.0**	1.2	1.2	0.9	0.5	0.5	0.5	0.5	1	1	0.5	1	1	0.545053	0.455030
$\frac{\pi}{4}$	0.6	0.8	**1.0**	1.2	0.9	0.5	0.5	0.5	0.5	1	1	0.5	1	1	0.505625	0.495548
$\frac{\pi}{4}$	0.6	0.8	**0.8**	1.2	0.9	0.5	0.5	0.5	0.5	1	1	0.5	1	1	0.450595	0.549974
$\frac{\pi}{4}$	0.6	0.8	1.2	**1.0**	0.9	0.5	0.5	0.5	0.5	1	1	0.5	1	1	0.551439	0.451251
$\frac{\pi}{4}$	0.6	0.8	1.2	**0.8**	0.9	0.5	0.5	0.5	0.5	1	1	0.5	1	1	0.552911	0.450789
$\frac{\pi}{4}$	0.6	0.8	1.2	1.2	**1.0**	0.5	0.5	0.5	0.5	1	1	0.5	1	1	0.5507	0.45084
$\frac{\pi}{4}$	0.6	0.8	1.2	1.2	**1.1**	0.5	0.5	0.5	0.5	1	1	0.5	1	1	0.550719	0.450822
$\frac{\pi}{4}$	0.6	0.8	1.2	1.2	0.9	**0.4**	0.5	0.5	0.5	1	1	0.5	1	1	0.549021	0.4511956
$\frac{\pi}{4}$	0.6	0.8	1.2	1.2	0.9	**0.3**	0.5	0.5	0.5	1	1	0.5	1	1	0.547656	0.452812
$\frac{\pi}{4}$	0.6	0.8	1.2	1.2	0.9	0.5	**0.4**	0.5	0.5	1	1	0.5	1	1	0.562337	0.435665
$\frac{\pi}{4}$	0.6	0.8	1.2	1.2	0.9	0.5	**0.3**	0.5	0.5	1	1	0.5	1	1	0.6580044	0.38062
$\frac{\pi}{4}$	0.6	0.8	1.2	1.2	0.9	0.5	0.5	**0.4**	0.5	1	1	0.5	1	1	0.548785	0.451833
$\frac{\pi}{4}$	0.6	0.8	1.2	1.2	0.9	0.5	0.5	**0.3**	0.5	1	1	0.5	1	1	0.547339	0.452792
$\frac{\pi}{4}$	0.6	0.8	1.2	1.2	0.9	0.5	0.5	0.5	**0.4**	1	1	0.5	1	1	0.55074	0.450863
$\frac{\pi}{4}$	0.6	0.8	1.2	1.2	0.9	0.5	0.5	0.5	**0.3**	1	1	0.5	1	1	0.550825	0.450800
$\frac{\pi}{4}$	0.6	0.8	1.2	1.2	0.9	0.5	0.5	0.5	0.5	**1.1**	1	0.5	1	1	0.551201	0.450503
$\frac{\pi}{4}$	0.6	0.8	1.2	1.2	0.9	0.5	0.5	0.5	0.5	**1.2**	1	0.5	1	1	0.551726	0.450151
$\frac{\pi}{4}$	0.6	0.8	1.2	1.2	0.9	0.5	0.5	0.5	0.5	1	**1.1**	0.5	1	1	0.551201	0.450503
$\frac{\pi}{4}$	0.6	0.8	1.2	1.2	0.9	0.5	0.5	0.5	0.5	1	**1.2**	0.5	1	1	0.551726	0.450151
$\frac{\pi}{4}$	0.6	0.8	1.2	1.2	0.9	0.5	0.5	0.5	0.5	1	1	**0.4**	1	1	0.557937	0.449148
$\frac{\pi}{4}$	0.6	0.8	1.2	1.2	0.9	0.5	0.5	0.5	0.5	1	1	**0.3**	1	1	0.553716	0.438856